Electrophoretic Time-of-Flight Measurements of Single DNA Molecules with Two Stacked Nanopores

ARTICLE *in* NANO LETTERS · NOVEMBER 2011

Impact Factor: 13.59 · DOI: 10.1021/nl2030079 · Source: PubMed

4 AUTHORS, INCLUDING:

Daniel Pedone
Technische Universität München
13 PUBLICATIONS **413** CITATIONS
SEE PROFILE

Friedrich C Simmel
Technische Universität München
139 PUBLICATIONS **4,997** CITATIONS
SEE PROFILE

Ulrich Rant
Dynamic Biosensors GmbH
57 PUBLICATIONS **1,256** CITATIONS
SEE PROFILE

NANO LETTERS

LETTER

pubs.acs.org/NanoLett

Electrophoretic Time-of-Flight Measurements of Single DNA Molecules with Two Stacked Nanopores

Martin Langecker,[†,‡] Daniel Pedone,[‡] Friedrich C. Simmel,[*,†] and Ulrich Rant[*,‡]

[†]Lehrstuhl für Bioelektronik, Physik-Department and ZNN/WSI, Technische Universität München, Am Coulombwall 4a, 85748 Garching, Germany

[‡]Walter-Schottky-Institut and Institute of Advanced Study, Technische Universität München, Am Coulombwall 4, 85748 Garching, Germany

Supporting Information

ABSTRACT: Electrophoretic transport through a solid-state nanodevice comprised of two stacked nanopore sensors is used to determine the free-solution mobility of DNA molecules based on their "time-of-flight" between the two pores. Mobility measurements are possible at very low (100 pM) DNA concentration and for low as well as high salt concentrations (here 30 mM and 1 M KCl). The mechanism of DNA transport through the device is elucidated by statistical analysis, showing the free-draining nature of the translocating DNA polymers and a barrier-dominated escape through the second pore. Furthermore, consecutive threading of single molecules through the two pores can be used to gain more detailed information on the dynamics of the molecules by correlation analysis, which also provides a direct electrical proof for translocation.

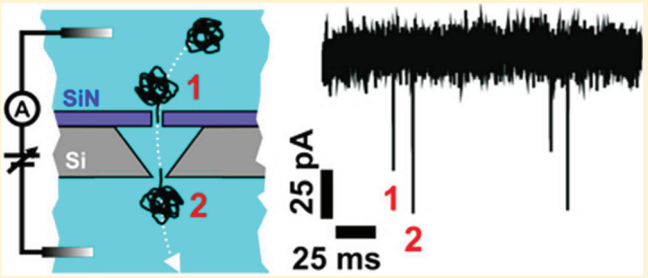

KEYWORDS: Nanopore, time-of-flight, DNA, mobility, zeta potential, translocation

In recent years, the blockage of ionic current caused by the translocation of single molecules through nanometer-sized holes has been utilized as a promising single molecule biosensor concept. Among the many applications envisioned for these devices are single-molecule detection,[1,2] DNA sequencing,[3,4] investigation of molecular interactions,[5−8] and basic biophysical studies on the stability and kinetics of biomolecular complexes.[9−15] Besides nanopore experiments performed using naturally occurring protein pores such as α-hemolysin embedded in lipid bilayer membranes,[16] an increasing number of studies has utilized solid-state nanopore structures.[17] These are typically fabricated in silicon-based materials by a combination of a variety of etching or "drilling" techniques.[18−22]

We recently developed a solid-state device that consists of two stacked nanopores separated by a micrometer-sized pyramidal compartment (a "pore−cavity−pore" (PCP) device, see Figure 1a).[23] In contrast to single nanopore devices, the PCP architecture has extended sensing and manipulation capabilities; e.g., it can be used to electrophoretically trap single particles or macromolecules within the cavity and controllably release them with a voltage pulse. Both nanopores act as resistive pulse sensors, and therefore the effective electrical information collected from each molecule is doubled. Furthermore, correlations between signals obtained from the two pores can be used to gain additional information about the dynamics of the translocating molecules. In the present work, we apply the PCP device to determine the free-solution electrophoretic mobility of double-stranded DNA (dsDNA) molecules in the length range from 6−15 kbp. The mobility is derived from single molecule time-of-flight (TOF) measurements obtained from the time the DNA molecules take to travel from pore to pore. By analyzing the resulting TOF distributions, we can identify the influence of drift, diffusion, and barrier-dominated escape on the transport of DNA through the device.

Experimental Setup. A detailed description of the fabrication procedure of the device has been published previously.[24] Briefly, the PCP device is fabricated from a silicon wafer coated with a 50 nm thick silicon nitride (SiN) layer on each side. One nanopore (the SiN pore) is created in the top SiN layer by means of e-beam lithography and reactive ion etching. Then a wet chemical etching step is employed to create the cavity below. Finally, after an additional lithographic step, feedback controlled etching from the bottom is used to create a second nanopore (the Si pore) at the apex of the cavity. Nanopore sizes and pore-to-pore distance are both tunable by the choice of fabrication parameters. This procedure has been successfully employed to fabricate 22 working PCP devices up to now, two of which have been used for this work.

Data presented in this paper were collected with a PCP device with a SiN pore with a diameter of 28 nm, a Si pore with size

Received: August 29, 2011
Revised: October 4, 2011

   dx.doi.org/10.1021/nl2030079 | *Nano Lett.* XXXX, XXX, 000–000

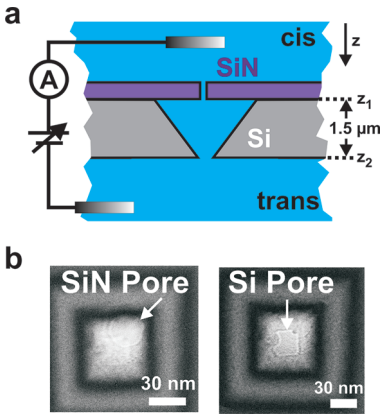

Figure 1. Measurement setup. (a) Schematic depiction of the pore−cavity−pore (PCP) device separating two electrolyte compartments electrically contacted with Ag/AgCl electrodes. A pyramidal microcavity embedded in silicon is connected to the cis side via a nanoscale pore in a 50 nm thick silicon nitride layer (SiN pore) and a second pore at its apex (Si pore). (b) Transmission electron micrographs showing the round SiN pore (left, diameter 28 nm) and the rectangular Si pore (right, 23 × 23 nm). Arrows indicate pores.

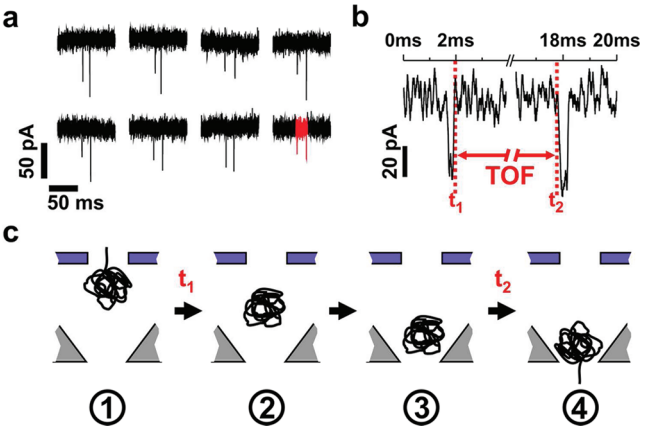

Figure 2. (a) Eight current blockade pairs detected in a representative 4 s current−time trace after addition of 100 pM of 10 kbp dsDNA to the cis side of the PCP device at a bias voltage of 300 mV. Equally spaced current spikes indicate sequential DNA translocation through the two nanopores of the PCP device. (b) Magnified view of the region marked in (a). We define the time difference between the rising edge of the first blockade and the falling edge of the second as the time-of-flight (TOF) of the molecule traversing the cavity. (c) Schematic depiction of the passage of a DNA molecule through the PCP device in four steps: (1) completed translocation through the first pore (t_1) accompanied by rapid recoiling; (2) electrophoretic transport toward the second pore; (3) jammed state at the entrance of the second pore; (4) threading into the second pore after successful chain-end localization (t_2) (see below, Broadening Mechanisms section).

23 × 23 nm (cf. Figure 1b), and a pore-to-pore distance of 1.5 μm (another PCP device has been used for the measurements presented in the Supporting Information). For translocation measurements, a bias potential was applied across the device via Ag/AgCl electrodes placed in two electrolyte compartments separated by the chip (cf. Figure 1a) and the current was monitored using a patch-clamp amplifier (Molecular Devices Axopatch 200B). The buffer electrolyte was 1 M KCl, 10 mM Tris, 1 mM EDTA, pH = 8, and all experiments were performed at room temperature.

Time of Flight Experiments. Upon addition of 10 kbp long dsDNA molecules (c = 100 pM) to the cis side of the device, typically a series of spikes in the current traces is observed. These temporary current blockades arise from single molecules translocating through either one of the two nanopores of the PCP device. Each nanopore hence works as a conventional resistive pulse sensor.[25] However, as the DNA molecules sequentially have to pass the two pores, the current spikes are correlated. As shown in Figure 2a, for sufficiently low analyte concentrations, resistive pulses are typically observed as isolated pairs. We assign the first pulse of each pair to the molecule's passage through the SiN pore, while the second pulse—under our experimental conditions delayed by 5−50 ms—is assigned to its subsequent translocation through the Si pore. Importantly, the presence of the second peak provides direct experimental evidence that the molecule causing the resistive pulses has actually translocated through the first pore and has not left the pore region to the cis side again.[16] While for conventional nanopore devices such evidence is only available via dedicated measurements that probe the dependence of translocation time on the length of the molecule[26] or that utilize optical tweezers,[27,28] the PCP device provides this proof "on the fly" for any single molecule measurement that is performed. This could be especially valuable for analytes like proteins.[29] In our experiments, we were able to assign 94% of all detected resistive pulses unambiguously to pairs. The remaining 6% were due to two or more pulse pairs that were too close to each other to allow for an unambiguous correlation.

Another important observation is that even for high voltages applied across the device the paired peaks did not merge into a single prolonged event, which would indicate that an elongated DNA molecule is present in both pores simultaneously. In principle, 10 kbp dsDNA with a contour length of 3.4 μm, could span the distance between the two pores (which is 1.5 μm). However, the presence of the two peaks shows that the DNA strands recoil during their passage between the pores. This is reasonable as simulations show that the electric field rapidly decreases within the cavity (Supporting Information) and therefore also the electrophoretic velocity. Hence, after passing the pore, the leading segment of the DNA molecule slows down immediately while successive segments are still being accelerated. This leads to instantaneous recoiling of the molecule. Furthermore, the Zimm relaxation time $\tau_z = \eta R^3/(2(3\pi)^{1/2}k_BT)$ (where η is the viscosity of water and R is the average end-to-end distance of the polymer)[30]—as a measure for the maximum recoiling time—for 10 kbp DNA is ≈7 ms.

For further analysis of the translocation process, we determined the interval between the end of a current blockade and the onset of the subsequent blockade for all pulses (see Figure 2b). The resulting distribution of time intervals exhibits a single peak in the range of 5−50 ms and represents the molecules' time-of-flight between the pores. By excluding times much longer than the peak of the distribution, we can identify all pairs of resistive pulses and assign each pulse to a translocation event through the first or the second pore (cf. Supporting Information).

Distribution of TOF as a Function of Voltage. In Figure 3a, representative TOF distributions are shown for four different bias voltages. The distributions are skewed, but their asymmetry decreases with increasing bias voltage. Such distributions are well-known from chromatography, and in fact the "exponentially

dx.doi.org/10.1021/nl2030079 |Nano Lett. XXXX, XXX, 000–000

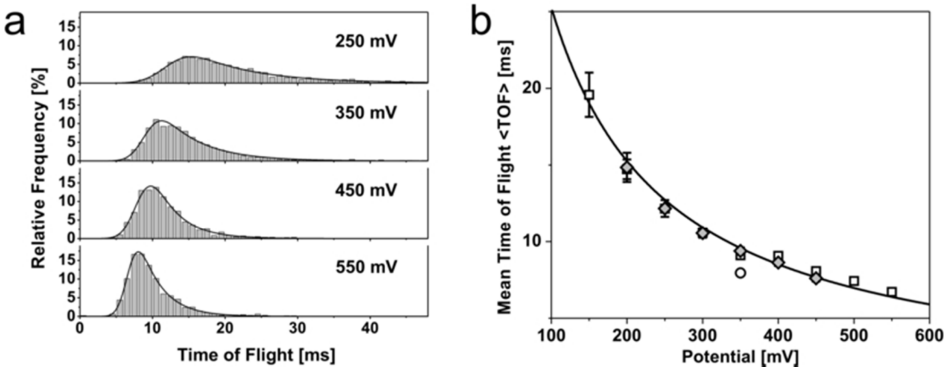

Figure 3. (a) TOF distribution for 10 kbp DNA at different bias voltages. The solid lines represent numerical fits with an exponentially modified Gaussian (EMG) model, from which the mean times of flight (plotted in (b)) are extracted. (b) Mean time-of-flight versus bias potential V for 6 kbp (gray diamonds), 10 kbp (hollow squares), and 15 kbp (hollow circles) DNA molecules. The solid line represents a numerical fit with an inverse voltage dependence (TOF $\sim V^{-1}$) (see text).

modified Gaussian" (EMG) used for chromatographic peak analysis fits our data remarkably well.[31] The EMG distribution phenomenologically accounts for several broadening mechanisms: diffusive motion, inhomogeneous flow paths, and fast mass transfer processes lead to a symmetric broadening of the TOF distribution around the mean value, which is accounted for by a Gaussian distribution. Additional processes with slow (first order) kinetics such as adsorption lead to asymmetric broadening, which is modeled by an exponential distribution. The EMG distribution is given by the convolution of these contributions

$$\mathrm{EMG}(t) = \frac{A}{\sqrt{2\pi}\sigma}\int_0^t \exp\left(-\frac{(t'-t_G)^2}{2\sigma^2}\right)\exp\left(-\frac{t-t'}{\tau}\right)\mathrm{d}t' \quad (1)$$

Fitting of this distribution to our data results in three fit parameters: the center of the Gaussian t_G, which we identify with the mean time-of-flight $\langle\mathrm{TOF}\rangle$ of the molecules; its width σ, characterizing the extent of diffusive broadening; the kinetic rate constant $k = \tau^{-1}$. The latter can be interpreted as a Kramers escape rate from the cavity, as will be discussed below.

Electrophoretic Mobility of DNA. In Figure 3b, the TOF values obtained from the EMG fits are shown as a function of bias voltage. These can be related to the electrophoretic mobility in the following manner. For a charged molecule in solution moving in an electric field E in direction z, the velocity is given by $v = \mathrm{d}z/\mathrm{d}t = \mu E$, where μ is the electrophoretic mobility. As the electric field inside the cavity of the device is not homogeneous (Supporting Information), the TOF is related to the electric field via the expression

$$\langle\mathrm{TOF}\rangle = \int_{t_{in}}^{t_{out}} \mathrm{d}t = \frac{1}{\mu}\int_{z_1}^{z_2}[E(z)]^{-1}\,\mathrm{d}z \quad (2)$$

where the integral is performed from the cavity's entrance z_1 to its exit z_2 (see Figure 1a). (The spatial extension of the molecule is not taken into account for the bounds of the integral. As $E(z)$ is large in the vicinity of the pores, choosing alternative bounds $z^*_{1,2} = z_{1,2} \pm R_g$ only has minor influence on the result (see supplementary Figure 1b, Supporting Information).) The electric field scales linearly with the applied bias voltage V. We can therefore introduce a reduced electric field $\epsilon(z) = E(z)/V$, which depends only on the geometry of the cavity and has the dimension of a length. Hence, we expect an indirect proportionality between the $\langle\mathrm{TOF}\rangle$ and V of the form $\langle\mathrm{TOF}\rangle(V) = \alpha/V$, which is very well fulfilled by our experimental data.

The proportionality factor is given by $\alpha = (1/\mu)\int_{z_1}^{z_2}[\epsilon(z)^{-1}]\,\mathrm{d}z$. This factor can be obtained from a fit to the data displayed in Figure 3a, which results in $\alpha = 0.4 \times 10^{-2}$ V s. On the other hand, we can numerically calculate the integral $\int_{z_1}^{z_2}[\epsilon(z)^{-1}]\,\mathrm{d}z$ using the electric field distribution within the cavity known from finite element calculations (see Supporting Information), which yields 77.6 $\mu\mathrm{m}^2$. Hence, the electrophoretic mobility for 10 kbp long DNA is obtained as $\mu = 1.8 \times 10^4\ \mu\mathrm{m}^2/(\mathrm{V\,s})$, which agrees well with mobility measurements performed in bulk using laser Doppler electrophoresis ($\mu = 2.3 \times 10^4\ \mu\mathrm{m}^2/(\mathrm{V\,s})$, see Supporting Information).

From measurements performed on 6 kbp long DNA, we obtained essentially the same TOF data and hence the same mobilities as for 10 kbp DNA (Figure 3a). This reflects the well-known free-draining nature of long dsDNA, resulting in a free-solution electrophoretic mobility that is independent of molecular weight for DNA molecules longer than ≈400 bp.[32] For 15 kbp DNA, the $\langle\mathrm{TOF}\rangle$ value is substantially lower, resulting in a higher mobility value of $2.8 \times 10^4\ \mu\mathrm{m}^2/(\mathrm{V\,s})$. This observation is consistent with an analysis of the molecule's conformational dynamics inside the device (see below), suggesting that the molecule does not relax completely before reaching the second pore.

In principle, the mobility values can also be used to determine the zeta potential of the transclocating molecules. Using the Helmholtz−Smoluchowski equation $\zeta = \mu\eta/\epsilon_0\epsilon_r$,[33] where η and ϵ_r are the viscosity and permittivity of water, respectively, we obtain $\zeta = -22.6$ mV for 10 kbp DNA at 1 M KCl, assuming a spherical conformation of the DNA molecule. We also performed measurements at lower ionic strength (30 mM KCl, resulting in a higher electrophoretic mobility) and found good agreement with previously published results on DNA mobility (see Supporting Information).

Broadening Mechanisms. The symmetric broadening of the TOF distributions can be well explained by diffusion. The average velocity in the z direction of a molecule traversing the device is given by $\bar{v} = d/\langle\mathrm{TOF}\rangle$, where d is the pore−pore distance. In the presence of diffusion, the variance of the distance traveled in time t is given by $(\Delta z)^2 = 2Dt$, where D is the diffusion

dx.doi.org/10.1021/nl2030079 |Nano Lett. XXXX, XXX, 000–000

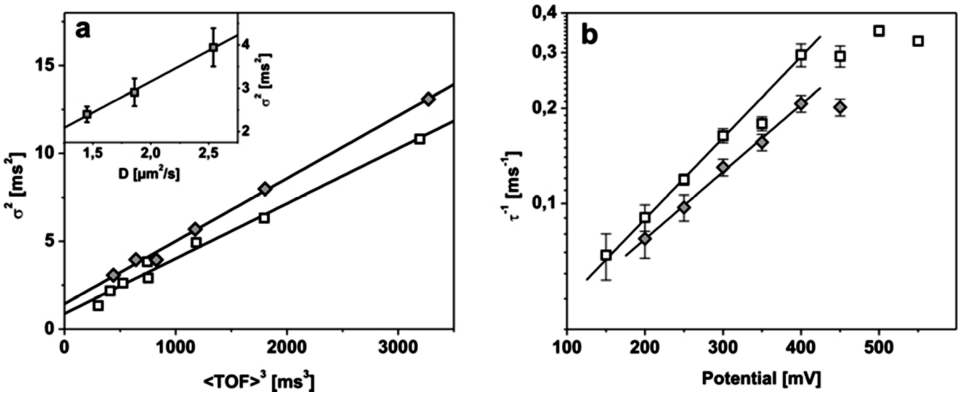

Figure 4. Broadening mechanisms. (a) Variance σ^2 of the Gaussian part of the EMG fit versus $\langle TOF \rangle^3$ for 10 kbp (hollow squares) and 6 kbp (gray diamonds) DNA. The solid lines represent linear fits to the data. Inset: Variance σ^2 versus diffusion coefficient at a bias voltage of 350 mV for 6, 10, and 15 kbp molecules. The solid line represents a linear fit. (b) Escape rate $1/\tau$ as a function of the applied bias potential in a semilogarithmic plot for 10 kbp (hollow squares) and 6 kbp DNA (gray diamonds). The solid lines represent exponential fits to the data.

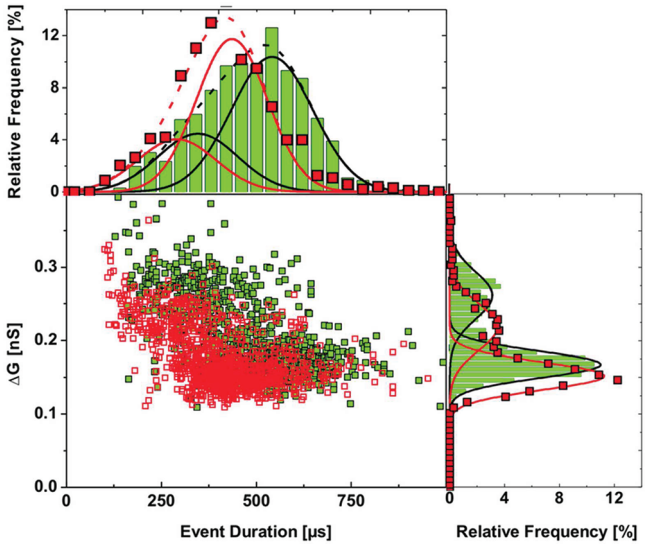

Figure 5. Scatter plot of the conductance blockade versus event duration for the translocation of 10 kbp DNA fragments through the SiN pore (red) and the Si pore (green) of the PCP device at a bias voltage of 200 mV. Each data point corresponds to a single translocation event. On the right and the top the corresponding histograms are shown. The lines correspond to Gaussian fits.

coefficient of the molecule. The variance in arrival times at the second pore can then be estimated as $\sigma^2 = \langle (t - \langle TOF \rangle)^2 \rangle \approx (\Delta z)^2/\bar{v}^2$,[34] or

$$\sigma^2 \approx \frac{2D}{d^2} \langle TOF \rangle^3 \qquad (3)$$

As shown in Figure 4a, the TOF variance obtained from the EMG fit for DNA molecules of lengths 6, 10, and 15 kbp follows the expected relationships $\sigma^2 \sim D$ and $\sigma^2 \sim \langle TOF \rangle^3$ remarkably well.

The asymmetric part of the EMG distribution, represented by the time constant, τ, is analyzed in Figure 5. τ^{-1} increases exponentially with the potential over a wide range of voltages, which suggests that the zasymmetric broadening is caused by voltage-activated escape over a free energy barrier. A similar behavior for DNA translocation through nanoscale pores was previously found by Wanunu et al.[35] In ref [36] a theoretical model was developed, in which the free energy barrier for translocation was attributed to two contributions—one due the localization of one of the DNA ends close to the pore entrance and the other caused by the DNA molecule's confinement inside the pore. The model predicts an increase of the escape rate with increasing DNA length, which is also in agreement with our results.

In previous experiments, we studied the escape of nanoparticles from an unbiased PCP device.[23] In this case the escape process was governed by the confinement inside the cavity and the diffusive motion of the particle. By contrast, we here observe directed motion toward the second pore (due to the applied electric field) and a barrier-dominated escape (due to the DNA molecule's conformation and its large size compared to the small pore diameter).

By analyzing TOF distributions, the escape process can be investigated uncoupled from diffusion and independent from analyte concentration, while in conventional nanopore experiments the mechanism of pore entry can only be accessed experimentally via the capture rate, which represents a combination of diffusion, drift, and barrier escape.

Influence of DNA Conformation. A unique feature of the PCP device is the possibility to correlate the translocation events detected by the two nanopores. In Figure 5, a scatter plot of the maximum conductance change ΔG versus event duration is shown for 10 kbp DNA translocations through the first and second pore, accompanied by the corresponding histograms. For both pores, these histograms exhibit a bimodal distribution, which can be fit by the sum of two Gaussian distributions.

We assign the lower conductance level to events, in which DNA translocates through the pores linearly, while the second conductance peak—mainly caused by multilevel events with a short-lived second level—is attributed to partially folded DNA. These types of translocation events have also been reported in previous publications on single nanopores of comparable size.[26,37] The different mean conductance changes and dwell times for the first (SiN) and the second (Si) pore are easily explained by the differences in pore dimensions and geometry (see Supporting Information). Moreover, the dwell time variance for the unfolded events is comparable for both pores (30% and 28% of the mean dwell time for the first and the second pore,

dx.doi.org/10.1021/nl2030079 |Nano Lett. XXXX, XXX, 000–000

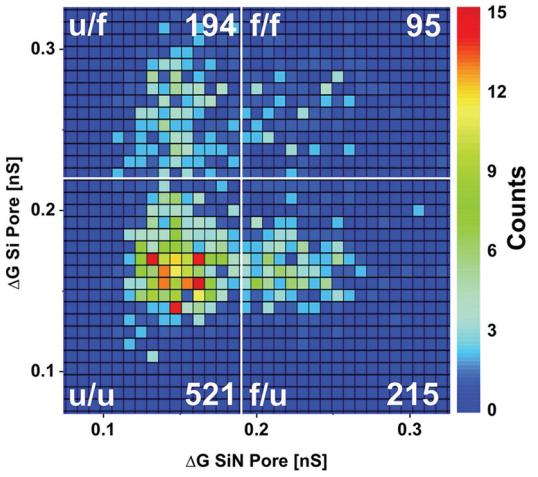

Figure 6. 2D histogram of the conductance change due Si pore translocation vs the corresponding conductance change due to subsequent Si pore translocation of 10 kbp DNA at 200 mV bias for a total of 1025 correlated event pairs. The color coding indicates the number of molecules for the corresponding ΔG values. The white lines separate areas attributed to events in which DNA translocated in a folded state from areas attributed to unfolded events. The total event count of each quadrant is shown in the corners.

respectively). This supports the assumption of instantaneous recoiling of "sufficiently short" molecules, as the variance in translocation time is known to be correlated to the initial conformation of the translocated molecules[38] and would therefore change if the molecule was (partially) linearized between the pores.

We also determined the blocked charge distributions for the two pores by integrating the blocked current over the dwell time (Supporting Information). The resulting distributions are unimodal and are very well fit by single Gaussian functions. This shows that the blocked charge is in fact independent of the folding state of the DNA, which is in agreement with previous studies.[26]

An important related question is whether the conformation of the DNA molecules arriving at the second pore is somehow affected by the first translocation event. To probe such an influence, we plotted a 2D histogram of the respective pore conductance changes (see Figure 6) for 10 kbp DNA at 200 mV bias voltage and divided it into four quadrants corresponding to the four possible combinations of folding states in the first and second pore, respectively: u/u, u/f, f/u, and f/f (f, folded; u, unfolded). In statistical terminology, this represents a 2×2 contingency table that can serve as the basis of a χ^2-test to probe the statistical independence of the events.[39] $\hat{\chi}^2$ can be calculated as follows:

$$\hat{\chi}^2 = \frac{n_{\text{total}}(n_{\text{uf}}n_{\text{fu}} - n_{\text{uu}}n_{\text{ff}})^2}{(n_{\text{uf}} + n_{\text{uu}})(n_{\text{ff}} + n_{\text{fu}})(n_{\text{uf}} + n_{\text{ff}})(n_{\text{uu}} + n_{\text{fu}})} \quad (4)$$

where n_{ij} is the frequency of the respective quadrant and n_{total} is the total number of events. The test yields $\hat{\chi}^2 = 1.318$, which confirms their independence for a significance level of 0.05. We performed this test for all 10 kbp DNA measurements in a range from 200 to 550 mV bias voltage, resulting in a mean $\hat{\chi}^2$ of 1.26 ± 0.98 with a maximum value of $\hat{\chi}^2_{\text{max}} = 2.56$ for the 400 mV measurement. Hence, statistically the folding state of the DNA at the second pore is not significantly altered due to its passage through the first pore. By way of contrast, measurements performed on 15 kbp DNA yielded a $\hat{\chi}^2$ value of 15.06, indicating that in this case the molecule's conformation still "remembers" its first translocation when entering the second pore. This means that—for a given pore-to-pore distance—for sufficiently long DNA molecules the previously stated assumption of instantaneous recoiling is not valid anymore. This could also explain the substantially lower TOF value for 15 kbp DNA. This type of correlation analysis is a unique feature of the PCP device. It may be also used, e.g., to detect modifications or conformational changes occurring during the traversal of the microcavity.

Discussion and Conclusion. We have demonstrated that a nanofabricated "pore−cavity−pore" device comprised of a pyramidal microcavity connected to its environment via two nanopore openings can be used for electrophoretic time-of-flight measurements on single DNA molecules of 6−15 kbp length. The experiments indicate that upon translocation of the DNA through the first pore, it immediately relaxes and traverses the cavity as in free-solution electrophoresis. Exit of the DNA from the cavity through the second pore is found to occur over a free energy barrier that is reduced with elevated voltages. The statistical distribution of the duration of the overall process is well-described by an exponentially modified Gaussian function. The different steps and time scales involved are summarized in Figure 2c.

As the electric field distribution within the pyramidal cavity can be accurately calculated, TOF (and, hence, velocity) measurements can be used to determine the free-solution mobility of the molecules. This in turn can be used to determine their ζ potential. In contrast to bulk methods, mobility measurements can be performed at very low analyte concentrations. In particular, they can be performed well below the polymer overlap concentration and therefore molecular or hydrodynamic interactions between polymer coils can be excluded. Furthermore, mobilities can be determined for higher salt concentrations than utilized in conventional zetasizers. This technique works for any charged analyte which is detectable upon translocation through the device's nanopores and can be especially valuable for analytes with a very low light scattering efficiency and no option for labeling. While we did not observe any indication of unspecific binding of the DNA molecules to the cavity surface, this might pose a problem for other analytes such as proteins,[40] in which case one would have to coat the surfaces with appropriate organosilanes.[41]

A particularly important feature of the PCP device is the possibility to assign resistive pulses to translocations through either the entry or exit pore of the cavity. This may be used for statistical correlation studies, e.g., to detect chemical or physical changes the molecules experience during traversal of the cavity or to filter out "bad" events from the data recordings. Combined with optical readout,[23] the PCP device can be turned into a unique tool for electrically controlled loading and manipulation of single molecules into a tailored microenvironment and for the study of biomolecular dynamics and biochemical processes under spatial confinement.

■ ASSOCIATED CONTENT

Supporting Information. Description of data processing, measurements of the DNA electrophoretic mobility at low ionic strength, simulations of the electric field inside the PCP device, "blocked charge" analysis of translocation events, and

dx.doi.org/10.1021/nl2030079 |Nano Lett. XXXX, XXX, 000–000

measurements of DNA diffusion coefficients and zeta potentials by dynamic light scattering. This material is available free of charge via the Internet at http://pubs.acs.org.

AUTHOR INFORMATION

Corresponding Author

*E-mail: simmel@ph.tum.de, rant@wsi.tum.de.

Author Contributions

M.L. and D.P. performed the experiments, D.P. and U.R. devised the experiments, M.L., D.P., F.C.S., and U.R. analyzed the experiments, and M.L. and F.C.S. wrote the paper.

ACKNOWLEDGMENT

We are very thankful to Robin Nagel for his help with the FEM simulations and to Marianne Hanzlik and Markus Döblinger for their help with TEM measurements. This work was supported by the DFG (SFB 863), BMBF (0312031) and through the Excellence Cluster Nanosystems Initiative Munich (NIM). M.L. gratefully acknowledges the support of the TUM Graduate School's Faculty Graduate Center Physics at the Technische Universität München.

REFERENCES

(1) Bayley, H.; Cremer, P. *Nature* **2001**, *413* (6852), 226–230.
(2) Howorka, S.; Siwy, Z. *Chem. Soc. Rev.* **2009**, *38* (8), 2360–2384.
(3) Branton, D.; Deamer, D. W.; Marziali, A.; Bayley, H.; Benner, S. A.; Butler, T.; Di Ventra, M.; Garaj, S.; Hibbs, A.; Huang, X. H.; Jovanovich, S. B.; Krstic, P. S.; Lindsay, S.; Ling, X. S. S.; Mastrangelo, C. H.; Meller, A.; Oliver, J. S.; Pershin, Y. V.; Ramsey, J. M.; Riehn, R.; Soni, G. V.; Tabard-Cossa, V.; Wanunu, M.; Wiggin, M.; Schloss, J. A. *Nat. Biotechnol.* **2008**, *26* (10), 1146–1153.
(4) Derrington, I. M.; Butler, T. Z.; Collins, M. D.; Manrao, E.; Pavlenok, M.; Niederweis, M.; Gundlach, J. H. *Proc. Natl. Acad. Sci. U.S.A.* **2010**, *107* (37), 16060–16065.
(5) Mathe, J.; Visram, H.; Viasnoff, V.; Rabin, Y.; Meller, A. *Biophys. J.* **2004**, *87* (5), 3205–3212.
(6) Renner, S.; Geltinger, S.; Simmel, F. C. *Small* **2010**, *6* (2), 190–194.
(7) Viasnoff, V.; Chiaruttini, N.; Bockelmann, U. *Eur. Biophys. J.* **2009**, *38* (2), 263–269.
(8) Vercoutere, W.; Winters-Hilt, S.; DeGuzman, V.; Deamer, D.; Ridino, S.; Rodgers, J.; Olsen, H.; Marziali, A.; Akeson, M. *Nucleic Acids Res.* **2003**, *31* (4), 1311–1318.
(9) Hornblower, B.; Coombs, A.; Whitaker, R. D.; Kolomeisky, A.; Picone, S. J.; Meller, A.; Akeson, M. *Nat. Methods* **2007**, *4* (4), 315–317.
(10) Tabard-Cossa, V.; Wiggin, M.; Trivedi, D.; Jetha, N. N.; Dwyer, J. R.; Marziali, A. *ACS Nano* **2009**, *3* (10), 3009–3014.
(11) Benner, S.; Chen, R. J. A.; Wilson, N. A.; Abu-Shumays, R.; Hurt, N.; Lieberman, K. R.; Deamer, D. W.; Dunbar, W. B.; Akeson, M. *Nat. Nanotechnol.* **2007**, *2* (11), 718–724.
(12) Cockroft, S. L.; Chu, J.; Amorin, M.; Ghadiri, M. R. *J. Am. Chem. Soc.* **2008**, *130* (3), 818–820.
(13) Stefureac, R. I.; Lee, J. S. *Small* **2008**, *4* (10), 1646–1650.
(14) Smeets, R. M. M.; Kowalczyk, S. W.; Hall, A. R.; Dekker, N. H.; Dekker, C. *Nano Lett.* **2009**, *9* (9), 3089–3095.
(15) Wanunu, M.; Sutin, J.; Meller, A. *Nano Lett.* **2009**, *9* (10), 3498–3502.
(16) Kasianowicz, J.; Brandin, E.; Branton, D.; Deamer, D. *Proc. Natl. Acad. Sci. U.S.A.* **1996**, *93* (24), 13770–13773.
(17) Dekker, C. *Nat. Nanotechnol.* **2007**, *2* (4), 209–215.
(18) Li, J.; Stein, D.; McMullan, C.; Branton, D.; Aziz, M.; Golovchenko, J. *Nature* **2001**, *412* (6843), 166–169.
(19) Storm, A. J.; Chen, J. H.; Ling, X. S.; Zandbergen, H. W.; Dekker, C. *Nat. Mater.* **2003**, *2* (8), 537–540.
(20) Chansin, G. A. T.; Mulero, R.; Hong, J.; Kim, M. J.; Demello, A. J.; Edel, J. B. *Nano Lett.* **2007**, *7*, 2901–2906.
(21) Wu, M. Y.; Smeets, R. M. M.; Zandbergen, M.; Ziese, U.; Krapf, D.; Batson, P. E.; Dekker, N. H.; Dekker, C.; Zandbergen, H. W. *Nano Lett.* **2009**, *9* (1), 479–484.
(22) Vlassiouk, I.; Apel, P. Y.; Dmitriev, S. N.; Healy, K.; Siwy, Z. S. *Proc. Natl. Acad. Sci. U.S.A.* **2009**, *106* (50), 21039–21044.
(23) Pedone, D.; Langecker, M.; Abstreiter, G.; Rant, U. *Nano Lett.* **2011**, *11* (4), 1561–1567.
(24) Pedone, D.; Langecker, M.; Muenzer, A. M.; Wei, R.; Nagel, R. D.; Rant, U. *J. Phys.: Condens. Matter* **2010**, *22* (45), 454115.
(25) Bayley, H.; Martin, C. R. *Chem. Rev.* **2000**, *100* (7), 2575–2594.
(26) Li, J. L.; Gershow, M.; Stein, D.; Brandin, E.; Golovchenko, J. A. *Nat. Mater.* **2003**, *2* (9), 611–615.
(27) Keyser, U. F.; Koeleman, B. N.; Van Dorp, S.; Krapf, D.; Smeets, R. M. M.; Lemay, S. G.; Dekker, N. H.; Dekker, C. *Nat. Phys.* **2006**, *2* (7), 473–477.
(28) Trepagnier, E.; Radenovic, A.; Sivak, D.; Geissler, P.; Liphardt, J. *Nano Lett.* **2007**, *7* (9), 2824–2830.
(29) Madampage, C. A.; Andrievskaia, O.; Lee, J. S. *Anal. Biochem.* **2010**, *396* (1), 36–41.
(30) Rubinstein, M.; Colby, R. H. *Polymer Physics*; Oxford University Press: Oxford and New York, 2003.
(31) Foley, J.; Dorsey, J. *J. Chromatogr. Sci.* **1984**, *22* (1), 40–46.
(32) Hoagland, D.; Arvanitidou, E.; Welch, C. *Macromolecules* **1999**, *32* (19), 6180–6190.
(33) Ohshima, H. *J. Colloid Interface Sci.* **1994**, *168* (1), 269–271.
(34) Lubensky, D. K.; Nelson, D. R. *Biophys. J.* **1999**, *77* (4), 1824–1838.
(35) Wanunu, M.; Morrison, W.; Rabin, Y.; Grosberg, A. Y.; Meller, A. *Nat. Nanotechnol.* **2010**, *5* (2), 160–165.
(36) Muthukumar, M. *J. Chem. Phys.* **2010**, *132* (19), 195101.
(37) Chen, P.; Gu, J.; Brandin, E.; Kim, Y. R.; Wang, Q.; Branton, D. *Nano Lett.* **2004**, *4* (11), 2293–2298.
(38) Lu, B.; Albertorio, F.; Hoogerheide, D. P.; Golovchenko, J. A. *Biophys. J.* **2011**, *101* (1), 70–79.
(39) Greenwood, P. E.; Nikulin, M. S. *A guide to chi-squared testing*; Wiley-Interscience: New York, 1996.
(40) Niedzwiecki, D. J.; Grazul, J.; Movileanu, L. *J. Am. Chem. Soc.* **2010**, *132* (31), 10816–10822.
(41) Wanunu, M.; Meller, A. *Nano Lett.* **2007**, *7* (6), 1580–1585.